bioRxiv preprint doi: https://doi.org/10.1101/2020.05.27.117184; this version posted May 27, 2020. The copyright holder for this preprint (which was not certified by peer review) is the author/funder, who has granted bioRxiv a license to display the preprint in perpetuity. It is made available under aCC-BY-NC-ND 4.0 International license.

Morphological Cell Profiling of SARS-CoV-2 Infection Identifies Drug Repurposing Candidates for COVID-19

Carmen Mirabelli[1,*], Jesse W. Wotring[2,*], Charles J. Zhang[2,†], Sean M. McCarty[2,†], Reid Fursmidt[3,†], Namrata S. Kadambi[3], Anya T. Amin[3], Teresa R. O'Meara[1], Carla D. Pretto[1], Tristan Frum[5], Jason R. Spence[3,5], Konstantinos D. Alysandratos[6,7], Jessie Huang[6,7], Darrell N. Kotton[6,7], Christiane E. Wobus[1], Kevin J. Weatherwax[4,8,9], George A. Mashour[4,8,10], Samuel K. Handelman[3,4], Matthew J. O'Meara[11], Jonathan Z. Sexton[2,3,4,8]

[1]Department of Microbiology and Immunology, University of Michigan Medical School, Ann Arbor, MI, 48109, USA
[2]Department of Medicinal Chemistry, College of Pharmacy, University of Michigan, Ann Arbor, MI, 48109, USA
[3]Department of Internal Medicine, Gastroenterology, Michigan Medicine at the University of Michigan, Ann Arbor, MI, 48109, USA
[4]U-M Center for Drug Repurposing, University of Michigan, Ann Arbor, MI, 48109, USA
[5]Department of Cell and Developmental Biology, University of Michigan, Ann Arbor, MI, 48109, USA
[6]Center for Regenerative Medicine of Boston University and Boston Medical Center, Boston, MA, 02118, USA
[7]The Pulmonary Center and Department of Medicine, Boston University School of Medicine, Boston, MA, 02118, USA
[8]Michigan Institute for Clinical and Health Research (MICHR), University of Michigan, Ann Arbor, MI, 48109, USA
[9]College of Pharmacy, University of Michigan, Ann Arbor, MI 48109, USA
[10]Department of Anesthesiology, Michigan Medicine at the University of Michigan, Ann Arbor, MI, 48109, USA
[11]Department of Computational Medicine and Bioinformatics, University of Michigan, Ann Arbor, MI, 48109, USA

[*]These authors contributed equally to this work.
[†]These authors contributed equally to this work.

Abbreviations:

MOI: multiplicity of infection
UMAP: uniform manifold approximation and projection
COVID-19: Coronavirus Disease-2019
MOA: mechanism of action
ROI: region of interest
iAEC2: induced pluripotent stem cell (iPSC)-derived alveolar epithelial type 2 cells
HCQ: hydroxychloroquine

Conflicts of interest

Jonathan Sexton is the co-founder of Verge Therapeutics, Inc. and owner of Curl Bio, LLC.

bioRxiv preprint doi: https://doi.org/10.1101/2020.05.27.117184; this version posted May 27, 2020. The copyright holder for this preprint (which was not certified by peer review) is the author/funder, who has granted bioRxiv a license to display the preprint in perpetuity. It is made available under aCC-BY-NC-ND 4.0 International license.

ABSTRACT

The global spread of the severe acute respiratory syndrome coronavirus 2 (SARS-CoV-2), and the associated disease COVID-19, requires therapeutic interventions that can be rapidly translated to clinical care. Unfortunately, traditional drug discovery methods have a >90% failure rate and can take 10-15 years from target identification to clinical use. In contrast, drug repurposing can significantly accelerate translation. We developed a quantitative high-throughput screen to identify efficacious single agents and combination therapies against SARS-CoV-2. Quantitative high-content morphological profiling was coupled with an AI-based machine learning strategy to classify features of cells for infection and stress. This assay detected multiple antiviral mechanisms of action (MOA), including inhibition of viral entry, propagation, and modulation of host cellular responses. From a library of 1,441 FDA-approved compounds and clinical candidates, we identified 15 dose-responsive compounds with antiviral effects. In particular, we discovered that lactoferrin is an effective inhibitor of SARS-CoV-2 infection with an IC_{50} of 308 nM and that it potentiates the efficacy of both remdesivir and hydroxychloroquine. Lactoferrin also stimulates an antiviral host cell response and retains inhibitory activity in iPSC-derived alveolar epithelial cells. Given its safety profile in humans, these data suggest that lactoferrin is a readily translatable therapeutic adjunct for COVID-19. Additionally, several commonly prescribed drugs were found to exacerbate viral infection and warrant clinical investigation. We conclude that morphological profiling for drug repurposing is an effective strategy for the selection and optimization of drugs and drug combinations as viable therapeutic options for COVID-19 pandemic and other emerging infectious diseases.

MAIN

SARS-CoV-2 is an enveloped, positive-sense, single-stranded RNA beta-coronavirus that emerged in Wuhan, China in November 2019 and rapidly developed into a global pandemic. The associated disease, COVID-19, has an array of symptoms, ranging from flu-like illness and

bioRxiv preprint doi: https://doi.org/10.1101/2020.05.27.117184; this version posted May 27, 2020. The copyright holder for this preprint (which was not certified by peer review) is the author/funder, who has granted bioRxiv a license to display the preprint in perpetuity. It is made available under aCC-BY-NC-ND 4.0 International license.

gastrointestinal distress[1,2] to acute respiratory distress syndrome, heart arrhythmias, strokes, and death[3,4]. Drug repurposing has played an important role in the search for COVID-19 therapies. Recently, the FDA issued emergency approval of remdesivir (GS-5734), a prodrug of a nucleoside inhibitor developed for Ebola virus treatment[5], and hydroxychloroquine, an aminoquinoline derivative first developed in the 1940s for the treatment of malaria, for patients with severe COVID-19. However, there are no established prophylactic strategies or direct antiviral treatments available to limit SARS-CoV-2 infections and to prevent/cure the associated disease COVID-19.

Repurposing of FDA-approved drugs is a promising strategy for identifying rapidly deployable treatments for COVID-19. Benefits of repurposing include known safety profiles, robust supply chains, and a short time-frame necessary for development[6]. Additionally, approved drugs serve as chemical probes to understand the biology of viral infection and can make new associations between COVID-19 and molecular targets/pathways that influence pathogenesis of the disease. A complementary approach to standard in vitro antiviral assays is high-content imaging-based morphological cell profiling. Using morphological cell profiling, it is possible to identify pathways and novel biology underlying infection, thus allowing for targeted screening around a particular biological process or targeting of host processes that limit viral infection. This enables the identification of multiple anti-viral mechanisms, allowing for the rational design of drug combinations or, conversely, revealing drugs that exacerbate infectivity or are associated with cytotoxicity.

Here, we developed a pipeline for quantitative high-throughput image-based screening of SARS-CoV-2 infection. We leveraged machine learning approaches to create an assay metric that accurately and robustly identifies features that predict antiviral efficacy and mechanism of action

bioRxiv preprint doi: https://doi.org/10.1101/2020.05.27.117184; this version posted May 27, 2020. The copyright holder for this preprint (which was not certified by peer review) is the author/funder, who has granted bioRxiv a license to display the preprint in perpetuity. It is made available under aCC-BY-NC-ND 4.0 International license.

(MOA). We identified several FDA-approved drugs and clinical candidates with unique antiviral activity. We further demonstrated that lactoferrin inhibits viral entry and replication, enhances antiviral host cell response, and potentiates the effects of remdesivir and hydroxychloroquine. Furthermore, we identified currently prescribed drugs that exacerbate viral infectivity. Collectively, we present evidence that morphological profiling can robustly identify new potential therapeutics against SARS-CoV-2 infection as well as drugs that potentially worsen COVID-19 outcomes.

Morphological profiling reveals unique features associated with SARS-CoV-2 infection

To determine the optimal cell line and appropriate endpoint for antiviral drug screening, we assessed SARS-CoV-2 infectivity in previously reported permissive cell lines: Vero-E6, Caco-2, and Huh-7[7]. Viral growth kinetics at a multiplicity of infection (MOI) of 0.2 revealed that Vero-E6, Caco2, and Huh-7 cells supported viral infection, with peak viral titers at 48 hours post infection (hrs p.i.) (Supplementary Figure 1A/B). Although the viral load was higher in Vero-E6 cells, Huh-7 were selected for our morphological drug screen as a human cell line that expresses both ACE2 and TMPRSS2, which are the primary entry factors for SARS-CoV-2[8]. Infection was detectable in Huh-7 cells at an MOI as low as 0.004 at 48 hrs p.i. (Supplementary Figure 1C), which highlights the high sensitivity of image-based screening. To identify compounds that inhibit or exacerbate infection, we selected an MOI of 0.2, leading to a baseline infectivity rate of 20%.

Morphological cell profiling was enabled through multiplexed staining and automated high-content fluorescence microscopy. Our multiplexed dye set included markers for SARS-CoV-2 nucleocapsid protein, nuclei (Hoechst 33342), neutral lipids (HCS LipidTox Green), and cell boundaries (HCS CellMask Orange). These fluorescent probes were chosen to capture a wide variety of cellular features relevant to viral infectivity, including nuclear morphology, nuclear

bioRxiv preprint doi: https://doi.org/10.1101/2020.05.27.117184; this version posted May 27, 2020. The copyright holder for this preprint (which was not certified by peer review) is the author/funder, who has granted bioRxiv a license to display the preprint in perpetuity. It is made available under aCC-BY-NC-ND 4.0 International license.

texture, cytoplasmic and cytoskeletal features, and indicators of cell health. From our initial profiling we observed three prominent morphological features associated with SARS-CoV-2 infection: the formation of syncytia, increased nucleoli count (Supplementary Figure 1D), and cytoplasmic protrusions (Figure 1). These features, which are key indicators of SARS-CoV-2 infection in Huh-7, were used to generate our machine learning pipeline for antiviral drug discovery.

Machine learning identifies FDA-approved molecules with antiviral activity against SARS-CoV-2

To identify compounds with antiviral activity against SARS-CoV-2, we screened a custom library of 1,441 FDA-approved compounds and rationally included clinical candidates in Huh-7 cells (Supplementary File 1). Compounds were assessed for their antiviral activity using a CellProfiler-based image analysis pipeline and a random forest classification algorithm to identify infected cells and quantify their morphological characteristics (Figure 2A). The random forest classifier leveraged 660 unique cellular features including measurements of intensity, texture and radial distribution for each fluorescent channel (nuclei, cytoplasm, lipid, virus). From the primary quantitative high-throughput screening (qHTS), hits were defined as compounds with consistent decreases in viral infectivity in at least three of the tested concentrations (50 nM, 250 nM, 500 nM, 1000 nM and 2000 nM) as well as minimal cytotoxicity. This approach for hit identification was intentionally designed to be broad to minimize false negatives and maximize our list of efficacious compounds which would later be refined. Our first-pass qHTS approach identified 132 compounds with moderate dose-responsive antiviral behavior between 50 nM and 2 μM, and successfully eliminated compounds without any significant activity or obvious cytotoxicity.

bioRxiv preprint doi: https://doi.org/10.1101/2020.05.27.117184; this version posted May 27, 2020. The copyright holder for this preprint (which was not certified by peer review) is the author/funder, who has granted bioRxiv a license to display the preprint in perpetuity. It is made available under aCC-BY-NC-ND 4.0 International license.

In confirmatory screening, 10-point, two-fold dilution dose-response experiments were performed in triplicate on the 132 qHTS hits, with validation of dose-responsive efficacy for 15 compounds below 1 μM potency (Supplementary Table 1 and Figure 2B). These hits include nine that are novel *in vitro* observations (lactoferrin, S1RA, entecavir, lomitapide, metoclopramide, bosutinib, thioguanine, fedratinib, and Z-FA-FMK), and six that have been previously identified to have antiviral activity (amiodarone, verapamil, gilteritinib, clofazimine[9,10], niclosamide[11], and remdesivir). In addition to antiviral drug hits, we also identified several compounds that appear to exacerbate SARS-CoV-2 infection, including trametinib, binimetinib and cobimetinib -potent MEK inhibitors used to treat metastatic melanoma- and the Parkinson's disease drugs carbidopa, methyldopa and levodopa (Supplementary Figure 2).

Cell level feature clustering reveals potential mechanisms of action for lead compounds

In contrast to standard single-endpoint *in vitro* assays, morphological cell profiling allows for the efficient visualization and quantitation of biological characteristics of viral infection and cytotoxicity. To assist with mechanistic determination, we used dimensionality reduction via the non-linear uniform manifold approximation and projection (UMAP) embedding, which projects the cellular feature vector into a 2-dimensional plot to observe clusters of cells based on their distinct morphological features[12]. Millions of cells were observed in the UMAP embedding through a range of drug concentrations alongside negative and positive controls to observe perturbations in specific morphological clusters (Supplementary Figure 3B).

In the UMAP embedding, we identified 15 regions of interest (ROI) with high cell density (Figure 3B). A broad density region (ROIs 10,15) contained uninfected cells with satellite populations having characteristic morphologies including cell division (ROI 6) and accumulation of lipids towards the periphery of the cell (ROI 12). A large disconnected region (ROIs 1-4) contained

bioRxiv preprint doi: https://doi.org/10.1101/2020.05.27.117184; this version posted May 27, 2020. The copyright holder for this preprint (which was not certified by peer review) is the author/funder, who has granted bioRxiv a license to display the preprint in perpetuity. It is made available under aCC-BY-NC-ND 4.0 International license.

individually infected cells (ROI 4), infected cells in syncytia (ROI 3), and cells adjacent to infected cells (ROIs 1,2) (Figure 3C). Pseudotime of the viral infection progression can be inferred through inspection of cluster populations where cells begin in the main cluster body (ROIs 10,15) and traverse to the infected cluster (ROIs 1-4) where there is punctate viral signal (ROI 1) which progress to isolated infected cells characterized by homogenous nucleocapsid staining throughout the cytoplasm (ROI 2), and ends with infection of surrounding cells and the formation of syncytia (ROIs 3,4). All efficacious compounds deplete ROIs 1-4 and thioguanine, clofazimine, S1RA and gilteritinib show differences in the UMAP cluster dynamics (Supplementary Figure 3B) suggestive of differing MOAs.

Lactoferrin blocks SARS-CoV-2 replication at different stages of the viral cycle

One of the most efficacious hits identified from our screen was lactoferrin, a protein found in milk and other secretory fluids[13]. We determined that lactoferrin has dose-dependent antiviral activity through a range of MOIs (Figure 4A and B). Previous work on lactoferrin in the context of infection with SARS-CoV-1 suggests that it blocks viral entry by binding heparan sulfate proteoglycans that are important for early viral attachment[13]. Our studies showed that lactoferrin blocks SARS-CoV-2 infection through entry inhibition and is also capable of rescuing infection when added 1 or 24 hrs p.i. (Figure 4B). Lactoferrin has been proposed to enhance innate interferon responses to limit viral replication within host cells[14]. Upon treatment, we observed a dose-dependent reduction of viral replication (Figure 4C), which was consistent with elevated mRNA levels of IFNβ and interferon-stimulated genes (ISG15, MX1, Viperin and IFITM3) in lactoferrin-treated Huh-7 cells (Figure 4D). Interestingly, we detected a robust antiviral effect by both holo and apolactoferrin, the latter being the component of widely available dietary supplements. To rule out a mode of action that involved a general iron depletion mechanism, we tested the protein transferrin and

bioRxiv preprint doi: https://doi.org/10.1101/2020.05.27.117184; this version posted May 27, 2020. The copyright holder for this preprint (which was not certified by peer review) is the author/funder, who has granted bioRxiv a license to display the preprint in perpetuity. It is made available under aCC-BY-NC-ND 4.0 International license.

found that it was devoid of any anti-SARS-CoV-2 activity at the highest concentration of 2.3 μM (Figure 4E). Lastly, we tested the efficacy of lactoferrin in physiologically relevant iPSC-derived alveolar epithelial type 2 cells (iAEC2s)[15,16]. Consistent with our findings in Huh-7 cells, pretreatment of iAEC2s with lactoferrin resulted in a significant reduction in the proportion of SARS-CoV-2 infected cells at MOI 10 (Figure 4F).

A clinically effective strategy for antiviral therapies uses a combinatorial (or "drug cocktail") approach, where compounds with varying MOAs are concomitantly used to target different stages in the viral life cycle and to minimize the risk of drug resistance from single-agent selective pressure. This is especially true for RNA viruses, which are highly variable and can develop drug-resistance[17]. Given the pronounced single-agent efficacy of lactoferrin, we tested whether combinations with remdesivir or hydroxycholoroquine could improve the overall antiviral activity. We found that lactoferrin potentiates the efficacy of both remdesivir (Figure 4G and Supplementary Figure 4A) and hydroxychloroquine (Figure 4H and Supplementary Figure 4B), which are currently explored treatments for SARS-CoV-2 infection. Therefore, combination therapy with lactoferrin could be beneficial in the management of the COVID-19 pandemic by reducing toxicity (e.g., hydroxycholorquine) or consumption (e.g., remdesivir).

DISCUSSION

In this study, we developed an experimental workflow based on high-content imaging and morphological profiling that allows for rapid screening of FDA-approved compounds, leveraging machine learning to determine potential MOA. We identified 15 FDA-approved compounds that limit SARS-CoV-2 infection *in vitro*. Of these, six were previously reported and serve as a benchmark validation of our endpoints and experimental approach, and nine were hitherto unknown. We demonstrate that this approach is versatile (i.e., it can be applied to both

bioRxiv preprint doi: https://doi.org/10.1101/2020.05.27.117184; this version posted May 27, 2020. The copyright holder for this preprint (which was not certified by peer review) is the author/funder, who has granted bioRxiv a license to display the preprint in perpetuity. It is made available under aCC-BY-NC-ND 4.0 International license.

transformed and more physiologically-relevant non-transformed cell lines) and can identify the emergent properties of the infection as well as novel phenotypes that can be perturbed through chemical inhibition.

A high-content morphological cell profiling approach is superior to image cytometry (tabulating percent positive) and plate reader assays for selecting and prioritizing drugs for repurposing. Here, viral staining is not merely an absolute measure for viral infection (or inhibition) but the starting point for a detailed investigation of infection trajectories and observations of numerous phenotypic targets, including inhibition of syncytia formation, viral entry, or viral replication, and modulation of the host cell. We report compounds with strong antiviral activity against SARS-CoV-2 and also their putative MOA.

The UMAP embedding was highly effective at visualizing the virally infected cell population and the progression of the viral infection trajectory was clearly visible. We gained insight into the putative antiviral MOAs via inspection of the cluster populations. For thioguanine and clofazimine, increasing concentrations appear to suppress isolated single infected cells (ROI 4) while a small number of syncytia (ROI 3) are still observable (Supplementary Figure 3B), suggesting a replication inhibition MOA. This observation is consistent with the established MOA of both drugs as inhibitors of nucleic acid synthesis[18,19]. S1RA reduces ROIs 1-4 evenly, but ROI 13 increases (Supplementary Figure 3B: S1RA) and is characterized by increased cytoplasmic nucleic acid staining (Supplementary Figure 3A: ROI 13), suggesting a host-modulation MOA. Lastly, gilteritinib demonstrates an increase in ROI 12 with treatment (Supplementary Figure 3B: gilteritinib), a cell cluster defined by large and distributed lipid accumulation (Supplementary Figure 3A: ROI 12). Lipid accumulation, in liver-derived Huh-7 cells, is associated with cytotoxicity and is consistent with reduction in viability with escalating dose (Figure 2B)[20].

bioRxiv preprint doi: https://doi.org/10.1101/2020.05.27.117184; this version posted May 27, 2020. The copyright holder for this preprint (which was not certified by peer review) is the author/funder, who has granted bioRxiv a license to display the preprint in perpetuity. It is made available under aCC-BY-NC-ND 4.0 International license.

Importantly, our study identified drugs that implicate new molecular targets/pathways in the pathogenesis of SARS-CoV-2 and produce clinically testable and readily translatable hypotheses. As an example, we observed a dose dependent antiviral activity of metoclopramide, a potent Dopamine Receptor D2 antagonist used to treat gastroesophageal reflux disease and prevent other gastrointestinal symptoms, including nausea and vomiting[21]. Gastrointestinal symptoms have been increasingly reported in more than half of the patients infected by SARS-CoV-2[2]. Notably, investigational drugs like hydroxychloroquine, lopinavir-ritonavir, tocilizumab and others can be associated with gastrointestinal and hepatic adverse events and hence are not ideal for patients already experiencing severe GI symptoms[22]. Metoclopramide therefore represents an interesting dual-target therapeutic option for COVID-19 patients. Interestingly, the pro-dopaminergic drugs carbidopa, levodopa, and methyldopa promote infection (Supplementary Figure 2), suggesting a dopamine-mediated contribution to viral entry or replication. Additionally, all MEK inhibitors exacerbated viral infection up to 300% indicating a causal role of MEK in SARS-CoV-2 pathogenesis. These *in vitro* observations should be validated through clinical research that examines whether concomitant presence of drug and SARS-CoV-2 exacerbates COVID-19.

As most FDA-approved drugs target human molecular targets, our screen helped identify crucial host factors involved in SARS-CoV-2 infection. Z-FA-FMK, an irreversible inhibitor of cysteine proteases, including cathepsins B, L, and S[23], exhibited potent antiviral activity. A recent report using a pseudovirus indicated cathepsin L is an entry factor of SARS-CoV-2[24]. The antiviral effect of Z-FA-FMK suggests that cathepsin L is a requirement also in the context of SARS-CoV-2 infection and suggests that this molecule could be a useful investigational tool to study virus entry. Similarly, fedratinib is an orally bioavailable semi-selective JAK2 inhibitor, approved by the FDA in 2019 for myeloproliferative neoplasm, a rare blood cancer that causes clotting and fibrosis[25]. JAK-inhibitors have been proposed for COVID-19 to specifically inhibit TH17-mediated inflammatory responses[26,27]. In addition, JAK-inhibitors have been proposed to block numb-

bioRxiv preprint doi: https://doi.org/10.1101/2020.05.27.117184; this version posted May 27, 2020. The copyright holder for this preprint (which was not certified by peer review) is the author/funder, who has granted bioRxiv a license to display the preprint in perpetuity. It is made available under aCC-BY-NC-ND 4.0 International license.

associated kinase responsible for clathrin-mediated viral endocytosis[28]. Several JAK-inhibitors are currently evaluated in clinical trials for COVID-19 management, including with baricitinib[29], jakotinib (ChiCTR2000030170), and ruxolitinib (ChiCTR2000029580). Further studies examining these Jak-inhibitors could serve as useful tools in the future to elucidate the involvement of the innate immune response in SARS-CoV-2 infection.

The sigma receptors (SigmaR1/R2) are permissive chaperones that mediate endoplasmic reticulum stress response and lipid homeostasis[30], processes that have been implicated in early stages of hepatitis C viral infection in Huh-7 cells[31] and coronavirus pathogenesis[32]. We identified two sigma receptor modulators amiodarone[33] (SigmaR1 IC_{50}: 1.4 nM, SigmaR2 IC_{50}: 1 nM), and S1RA[34] (E-52862; SigmaR1 IC_{50}: 17 nM antagonist, SigmaR2 IC_{50}: > 1 μM) with potent antiviral activity, demonstrating IC50 values of 52 nM and 222 nM, respectively, with limited cell toxicity. Amiodarone is approved for treatment of arrhythmias but, like hydroxychloroquine, has potent cardiotoxic side effects through inhibition of the hERG ion channel[35] that limit therapeutic potential. S1RA has completed phase II clinical trials for the treatment of neuropathic pain[36,37]. Although Gordon *et al.* identified several other sigmaR1/R2 modulators that inhibited SARS-CoV-2 infection in Vero-E6 cells, antiviral activity for S1RA was not observed[38]. This suggests that the activity of S1RA is dependent on host cell factors specific to each cell line and, promisingly, that human cells may be more responsive to this compound.

Most noteworthy, our screen demonstrates lactoferrin as a SARS-CoV-2 inhibitor *in vitro* with multimodal efficacy. We showed efficacy in multiple cell types, including a non-transformed and clinically relevant iPSC-derived model of alveolar epithelium. Lactoferrin gene expression has been shown previously to be highly upregulated in response to SARS-CoV-1 infection[39] and, in addition to enhancing natural killer cell and neutrophil activity, lactoferrin blocks viral entry through binding to heparan sulfate proteoglycans. Interestingly, lactoferrin retains anti-SARS-CoV-2

bioRxiv preprint doi: https://doi.org/10.1101/2020.05.27.117184; this version posted May 27, 2020. The copyright holder for this preprint (which was not certified by peer review) is the author/funder, who has granted bioRxiv a license to display the preprint in perpetuity. It is made available under aCC-BY-NC-ND 4.0 International license.

activity 24 hrs p.i., which suggests additional MOA other than simple entry inhibition. Although we cannot conclude a definitive and complete MOA, we show significant host cell modulation through increased expression of several interferon-stimulated genes upon treatment with lactoferrin. Additionally, lactoferrin has been previously shown to decrease the production of IL-6[40], which is one of the key players of the "cytokine storm" produced by SARS-CoV-2 infection[41,42]. Importantly, we found that lactoferrin retains activity in both the holo and apo forms, the latter being the component of orally available lactoferrin supplements. Orally available lactoferrin could be especially effective in mitigating the gastrointestinal symptoms that are present in COVID-19 patients[43]. The mechanisms may be similar to how lactoferrin reduces human norovirus infection through induction of innate immune responses[44], especially as lactoferrin gene polymorphisms are associated with increased susceptibility to infectious diarrhea[45]. If lactoferrin reduces viral load in the GI tract, it could reduce fecal-oral transmission of COVID-19[46].

Combination therapies are likely to be required for effectively treating SARS-CoV-2 infection, and this approach has already shown some promise. For example, combination therapy with interferon beta-1b, lopinavir–ritonavir, and ribavirin showed efficacy against SARS-CoV-2 in a prospective, open-label, randomized, phase 2 trial[47]. We demonstrated in our study that lactoferrin potentiates the antiviral activity of both remdesivir and hydroxychloroquine and could be used as a combination therapy with these drugs, which are currently being used or studied for the treatment of COVID-19. Due to its wide availability, limited cost and lack of adverse effects, lactoferrin could be a rapidly deployable option for both prophylaxis and the management of COVID-19.

Although our findings are promising, further studies are needed to confirm their efficacy in other representative *in vitro* cell lines and/or clinical studies. UMAP analysis provides limited insight to

bioRxiv preprint doi: https://doi.org/10.1101/2020.05.27.117184; this version posted May 27, 2020. The copyright holder for this preprint (which was not certified by peer review) is the author/funder, who has granted bioRxiv a license to display the preprint in perpetuity. It is made available under aCC-BY-NC-ND 4.0 International license.

MOA and serve as a basis for future pharmacological studies specific to our compounds in treatment of SARS-CoV-2. These studies are currently ongoing.

In conclusion, high-content morphological cell profiling for drug repurposing screening enabled the identification of both novel antivirals efficacious against SARS-CoV-2 and compounds that possibly exacerbate SARS-CoV-2 infection. Furthermore, in contrast to other drug repurposing studies, the assay reported here allowed for the identification of potential MOA, including host cell responses. This approach to preclinical testing has promise for identifying other anti-SARS-CoV-2 drugs, rationally designing therapeutic combinations with multiple MOAs, and deployment of these new combinations in a rapid and systemic fashion.

Supplementary Information is available for this paper.

Correspondence and requests for materials should be addressed to jzsexton@umich.edu

ACKNOWLEDGEMENTS

Funding: University of Michigan Institute for Clinical and Health Research (MICHR) (NCATS - UL1TR002240) and its Center for Drug Repurposing. JZS is supported by the National Institute of Diabetes and Digestive and Kidney Diseases (R01DK120623). JWW is supported by the pharmacological sciences training program (PSTP) T32 training grant. CM is supported by Marie-Slodowska Curie individual fellowship (GA - 841247) and MICHR Postdoctoral Translational Scholars Program. KDA is supported by the I.M. Rosenzweig Junior Investigator Award from the Pulmonary Fibrosis Foundation. JRS is supported by the National Heart, Lung, and Blood Institute (NHLBI – R01HL119215), by the NIAID Novel Alternative Model Systems for Enteric Diseases

bioRxiv preprint doi: https://doi.org/10.1101/2020.05.27.117184; this version posted May 27, 2020. The copyright holder for this preprint (which was not certified by peer review) is the author/funder, who has granted bioRxiv a license to display the preprint in perpetuity. It is made available under aCC-BY-NC-ND 4.0 International license.

(NAMSED) consortium (U19AI116482) and by grant number CZF2019-002440 from the Chan Zuckerberg Initiative DAF, an advised fund of Silicon Valley Community Foundation.

The authors would like to thank Matthew Chess for Amazon AWS support, Kevin Yan and Peyton Uhl at Yokogawa for imaging support, Nick Santoro at the University of Michigan Center for Chemical Genomics. We thank David Egan and Wienand Omta from Core Life Analytics for assisting high content data analytics as well as Philip Cheung and Brian Bolt at ReFactor Biosciences for assistance with HTS data registration. Finally, we thank Tracey Schultz and Dianne Jazdzyk for project management.

METHODS

Cells and Virus. Vero E6, Caco2 and Huh7 cells were maintained at 37°C with 5% CO2 in Dulbecco's Modified Eagle's Medium (DMEM; Welgene), supplemented with 10% heat-inactivated fetal bovine serum (FBS), HEPES, non-essential amino-acids, L-glutamine and 1X Antibiotic-Antimycotic solution (Gibco). iPSC (SPC2 iPSC line, clone SPC2-ST-B2, Boston University) derived alveolar epithelial type 2 cells (iAEC2s) were differentiated as previously described and maintained as alveolospheres embedded in 3D Matrigel in "CK+DCI" media, as previously described (Jacob et al. 2019). iAEC2s were passaged approximately every two weeks by dissociation into single cells via the sequential application of dispase (2mg/ml, Thermo Fisher Scientific, 17105-04) and 0.05% trypsin (Invitrogen, 25300054) and re-plated at a density of 400 cells/µl of Matrigel (Corning, 356231), as previously described (Jacob et al. 2019). SARS-CoV-2 WA1 strain was obtained by BEI resources and was propagated in Vero E6 cells. Viral titers were determined by TCID50 assays in Vero E6 cells (Reed and Muench method) by microscopic scoring. All experiments using SARS-CoV-2 were performed at the University of Michigan under Biosafety Level 3 (BSL3) protocols in compliance with containment procedures in laboratories

bioRxiv preprint doi: https://doi.org/10.1101/2020.05.27.117184; this version posted May 27, 2020. The copyright holder for this preprint (which was not certified by peer review) is the author/funder, who has granted bioRxiv a license to display the preprint in perpetuity. It is made available under aCC-BY-NC-ND 4.0 International license.

approved for use by the University of Michigan Institutional Biosafety Committee (IBC) and Environment, Health and Safety (EHS).

Viral Quantification. Vero E6, Caco2 and Huh7 cells were seeded in a 48-well plate at 2x10^4 cells/well incubated overnight at 37°C with 5% CO2. Cells were then infected with SARS-CoV-2 WA1 at a multiplicity of infection (MOI) of 0.2. One hour after infection, cells were harvested (day 0 of infection) or kept at 37°C for 1, 2 and 3 days p.i. Viral titer determination was performed by TCID50 assay on Vero E6 cells of the total virus (supernatant and intracellular fraction). Alternatively, cells were harvested with Trizol and total cellular and viral RNA was extracted with the ZymoGen Direct-zol RNA extraction kit. Viral RNA was quantified by RT-qPCR using the 2019-nCoV CDC qPCR Probe Assay and the probe set N1 (IDT technologies). IFNβ, viperin, MX1, ISG15, IFITM3 and the housekeeping gene GAPDH mRNA levels were quantified by qPCR with SsoAdvanced™ Universal SYBR® Green Supermix (Bio-Rad) with specific primers (IFNβ: F-TTGACATCCCTGAGGAGATTAAGC, R- TCCCACGTACTCCAACTTCCA; MX1: F-CCAGCTGCTGCATCCCACCC, R-AGGGGCGCACCTT CTCCTCA; ISG15: F-TGGCGGGCAACGAATT, R- GGGTGATCTGCGCCTTCA; IFITM3: F-TCCCAC GTACTCCAACTTCCA, R-AGCACCAGAAACACGTGCACT; GAPDH: F-CTCTGCTCCTCCTGTTCGAC, R-GCGCCCCACCAAGCTCAAGA). Fold increase was calculated by using the ΔΔCt method over non-infected untreated Huh-7.

Viral Infectivity Assay. 384-well plates (Perkin Elmer, 6057300) were seeded with Huh-7 cells at 3000 cells/well and allowed to adhere overnight. Compounds were then added to the cells and incubated for 4 hours. The plates were then transferred to BSL3 containment and infected with SARS-CoV-2 WA1 at a multiplicity of infection (MOI) of 0.2 in a 10 µL addition with shaking to distribute virus. After one hour of absorption, the virus inoculum was removed and media replaced with fresh compound. Uninfected cells and vehicle-treated cells were included as positive and

bioRxiv preprint doi: https://doi.org/10.1101/2020.05.27.117184; this version posted May 27, 2020. The copyright holder for this preprint (which was not certified by peer review) is the author/funder, who has granted bioRxiv a license to display the preprint in perpetuity. It is made available under aCC-BY-NC-ND 4.0 International license.

negative control, respectively. Two days post-infection, cells were fixed with 4% PFA for 30 minutes at room temperature, permeabilized with 0.3% Triton X-100 and blocked with antibody buffer (1.5% BSA, 1% goat serum and 0.0025% Tween 20). The plates were then sealed, surface decontaminated, and transferred to BSL2 for staining with the optimized fluorescent dye-set: anti-nucleocapsid SARS-CoV-2 antibody (Antibodies Online, Cat# ABIN6952432) overnight treatment at 4C followed by staining with secondary antibody Alexa-647 (goat anti-mouse, Thermo Fisher, A21235), Hoechst-33342 Pentahydrate (bis-Benzimide) for nuclei staining (Thermo FIsher, H1398), HCS LipidTOX™ Green Neutral Lipid Stain (Thermo Fisher, H34475), and HCS CellMask™ Orange for cell delineation (Thermo Fisher H32713). iAEC2 maintained in 3D culture were dissociated to single cells and seeded in collagen coated 384-well plates at a seeding density of 8000 cells/well in the presence of 10 μM Y-27632 for the first 48 hours after plating (APExBIO, A3008), and grown to confluence over 72 hours. The following infection, compound treatment, and fixing was identical to that of Huh-7. Staining protocol for the iAEC2s differed slightly with the addition of an anti-acetylated tubulin primary antibody (Cell Signaling, 5335), instead of HCS CellMask Orange, and the use of an additional secondary Alexa 488 antibody (donkey anti-rabbit, Jackson ImmunoResearch, 711-545-152).

Compound Library. The compound library deployed for drug screening was created using the FDA-Approved Drugs Screening Library (Item No. 23538) from Cayman Chemical Company. This library of 875 compounds was supplemented with additional FDA approved drugs and rationally included clinical candidates from other vendors including MedChemExpress, Sigma Aldrich, and Tocris. Our library was formatted in five 384-well compound plates and was dissolved in DMSO at 10 mM. Hololactoferrin (Sigma Aldrich, L4765), apolactoferrin (Jarrow Formulas, 121011) and transferrin (Sigma Aldrich, T2036) were handled separately and added manually in cell culture media. Dilution plates were generated for qHTS at concentrations of 2 mM, 1 mM, 500 μM, 250 μM and 50 μM.

bioRxiv preprint doi: https://doi.org/10.1101/2020.05.27.117184; this version posted May 27, 2020. The copyright holder for this preprint (which was not certified by peer review) is the author/funder, who has granted bioRxiv a license to display the preprint in perpetuity. It is made available under aCC-BY-NC-ND 4.0 International license.

qHTS Primary Screen and Dose Response Confirmation. For the qHTS screen, compounds were added to cells using a 50 nL pin tool Caliper Life Sciences Sciclone ALH 3000 Advanced Liquid Handling system at the University of Michigan Center for Chemical Genomics (CCG). Concentrations of 2 μM, 1 μM, 500 nM, 250 nM and 50 nM were included for the primary screen. Post qHTS screen, all compounds were dispensed using an HP D300e Digital Compound Dispenser and normalized to a final DMSO concentration of 0.1% DMSO. Confirmation dose response was performed in triplicate and in 10-point:2-fold dilution.

Imaging. Stained cell plates were imaged on both Yokogawa CQ1 and Thermo Fisher CX5 high content microscopes with a 20X/0.45NA LUCPlan FLN objective. Yokogawa CQ1 imaging was performed with four excitation laser lines (405nm/488nm/561nm/640nm) with spinning disc confocal and 100ms exposure times. Laser power was adjusted to yield optimal signal to noise ratio for each channel. Maximum intensity projection images were collected from 5 confocal planes with a 3 micron step size. Laser autofocus was performed and nine fields per well were imaged covering approximately 80% of the well area. The Thermofisher CX5 with LED excitation (386/23nm, 485/20nm, 560/25nm, 650/13nm) was also used and exposure times were optimized to maximize signal/background. Nine fields were collected at a single Z-plane as determined by image-based autofocus on the Hoechst channel. The primary qHTS screen was performed using CX5 images and all dose-response plates were imaged using the CQ1.

Image Segmentation and feature extraction. The open source CellProfiler software was used in an Ubuntu Linux-based distributed Amazon AWS cloud implementation for segmentation, feature extraction and results were written to an Amazon RDS relational database using MySQL. A pipeline was developed to automatically identify the nuclei, cell, cytoplasm, nucleoli, neutral

bioRxiv preprint doi: https://doi.org/10.1101/2020.05.27.117184; this version posted May 27, 2020. The copyright holder for this preprint (which was not certified by peer review) is the author/funder, who has granted bioRxiv a license to display the preprint in perpetuity. It is made available under aCC-BY-NC-ND 4.0 International license.

lipid droplets and syncytia for feature extraction. Multiple intensity features and radial distributions were measured for each object in each channel and cell size and shape features were measured. Nuclei were segmented using the Hoechst-33342 image and the whole cell mask was generated by expanding the nuclear mask to the edge of the Cell Mask Orange image.

Data Pre-Processing. Cell level data were pre-processed and analyzed in the open source Knime analytics platform[48]. Cell-level data was imported into Knime from MySQL, drug treatment metadata was joined and features were centered and scaled. Features were pruned for low variance (<5%) and high correlation (>95%) and resulted in 660 features per cell.

Statistical methods and hypothesis testing. Dose-response curves were fit and pairwise differences between experimental conditions were tested using Prism (Graphpad Software, San Diego, CA, USA). Other statistical tests were performed in the statistical programming language and environment R.

Machine Learning - Infectivity score and field-level scoring. Multiple logistic regression as implemented in the statistical language and environment R was used to identify features characteristic of cells within infected wells. Models were fit to cells from infected and uninfected control wells in the first five plate-series of the quantitative high throughput screen. As an independent benchmark, these logistic regression models were validated against a manually selected set of individual infected and uninfected cells; features which degraded performance on the benchmark were excluded from the model. The final model included only virus channel intensity features in the cell and cytoplasm ROIs. As a threshold for initial

bioRxiv preprint doi: https://doi.org/10.1101/2020.05.27.117184; this version posted May 27, 2020. The copyright holder for this preprint (which was not certified by peer review) is the author/funder, who has granted bioRxiv a license to display the preprint in perpetuity. It is made available under aCC-BY-NC-ND 4.0 International license.

classification, the minimum value from virus-infected cells in the benchmark was used; the final decision rule is given in Eq. 1.

(Eq.1) : A cell is infected if (Cells_Intensity_IntegratedIntensityEdge_Virus × 0.1487025 + Cells_Intensity_MeanIntensityEdge_Virus × -38.40196 + Cells_Intensity_MaxIntensityEdge_Virus × 42.70269 + Cytoplasm_Intensity_StdIntensity_Virus × 42.54849) ≥ 1.525285

Then, individual field images from the infected control were categorized as confirmed-infected when the mean feature values, across all cells in the field, were above the threshold in Eq. 1. Using mean values for all 660 cell-profiler features in each field, a random forest classifier was trained to predict a probability of membership in the category of uninfected control fields vs confirmed-infected fields. The output of this random forest classifier is reported as "Probpos" (for the positive, uninfected control), throughout. Field level mean/median feature values were computed and a random forest model was fit between the positive control (32 uninfected wells) and the negative control (32 infected wells, 0.1% DMSO vehicle treated) with 80/20 cross validation. The compound treated wells were scored with the RF model and the efficacy score was normalized to the individual plate.

UMAP embedding. The embed_umap application of MPLearn (v0.1.0, https://github.com/momeara/MPLearn) was used to generate UMAP embeddings. Briefly, each for a set of cells, each feature was per-plate standardized and jointly orthogonalized using sklearn.IncrementalPCA(n_components=379, batch_size=1000). Then features were embedded

bioRxiv preprint doi: https://doi.org/10.1101/2020.05.27.117184; this version posted May 27, 2020. The copyright holder for this preprint (which was not certified by peer review) is the author/funder, who has granted bioRxiv a license to display the preprint in perpetuity. It is made available under aCC-BY-NC-ND 4.0 International license.

into 2-dimensions using umap-learn (v0.4.1) (McInnes et al. 2018) with umap.UMAP(n_components=2, n_neighbors=15, min_dist=0, init='spectral', low_memory=True, verbose=True). Embeddings were visualized using Holovies Datashader (v1.12.7)[49], using histogram equalization and the viridis color map. Visualizing subsets was done in JMP Pro 14.

Data analytics. HC Stratominer (Core Life Analytics, Utrecht NL) was used as an independent method for hit-calling and performs fully automated/streamlined cell-level data pre-processing and score generation. IC Stratominer was also used to fit dose response curves for qHTS. Compound registration and assay data registration were performed using the open source ACAS platform (Refactor BioSciences github https://github.com/RefactorBio/acas).

Dose-response analysis and compound selection. In qHTS screening, a compound was selected to be carried forward into full dose response confirmation when meeting one of the following criteria: 1) Probpos greater than 0.75 for the median field in at least three concentrations, with per-field cell counts at least 60% of the positive control, and without an observed standard deviation in Probpos across-fields-in-the-well of 0.4 or greater, 2) a dose-response relationship with Probpos was observed (by inspection) across the five concentrations tested, including compounds with Propbos greater than 0.90 at the two highest concentrations, or 3) compounds of interest not meeting this criteria were carried forward if reported positive in the literature or were being evaluated in clinical trials for COVID-19.

Dose response analysis in the confirmation and combinatorial screening. Due to the spatial inhomogeneity of infected cells across a single well, approximately half of the fields were undersaturated, leading to a consistent distribution in Probpos that saturates in the top third of 27

bioRxiv preprint doi: https://doi.org/10.1101/2020.05.27.117184; this version posted May 27, 2020. The copyright holder for this preprint (which was not certified by peer review) is the author/funder, who has granted bioRxiv a license to display the preprint in perpetuity. It is made available under aCC-BY-NC-ND 4.0 International license.

rank-ordered fields (from 9 fields and triplicate wells) for each concentration tested. The Probpos effect for a compound concentration was tabulated by averaging the top third of rank ordered fields. Outlier fields with high Probpos values were visually inspected and eliminated if artifacts (segmentation errors or debris) were observed. Cells treated with known fluorescence drugs including Clofazimine, were confirmed to not have spectral interference. Dose response curves were fit with Graphpad Prism using a semilog 4-parameter variable slope model.

bioRxiv preprint doi: https://doi.org/10.1101/2020.05.27.117184; this version posted May 27, 2020. The copyright holder for this preprint (which was not certified by peer review) is the author/funder, who has granted bioRxiv a license to display the preprint in perpetuity. It is made available under aCC-BY-NC-ND 4.0 International license.

FIGURES AND LEGENDS

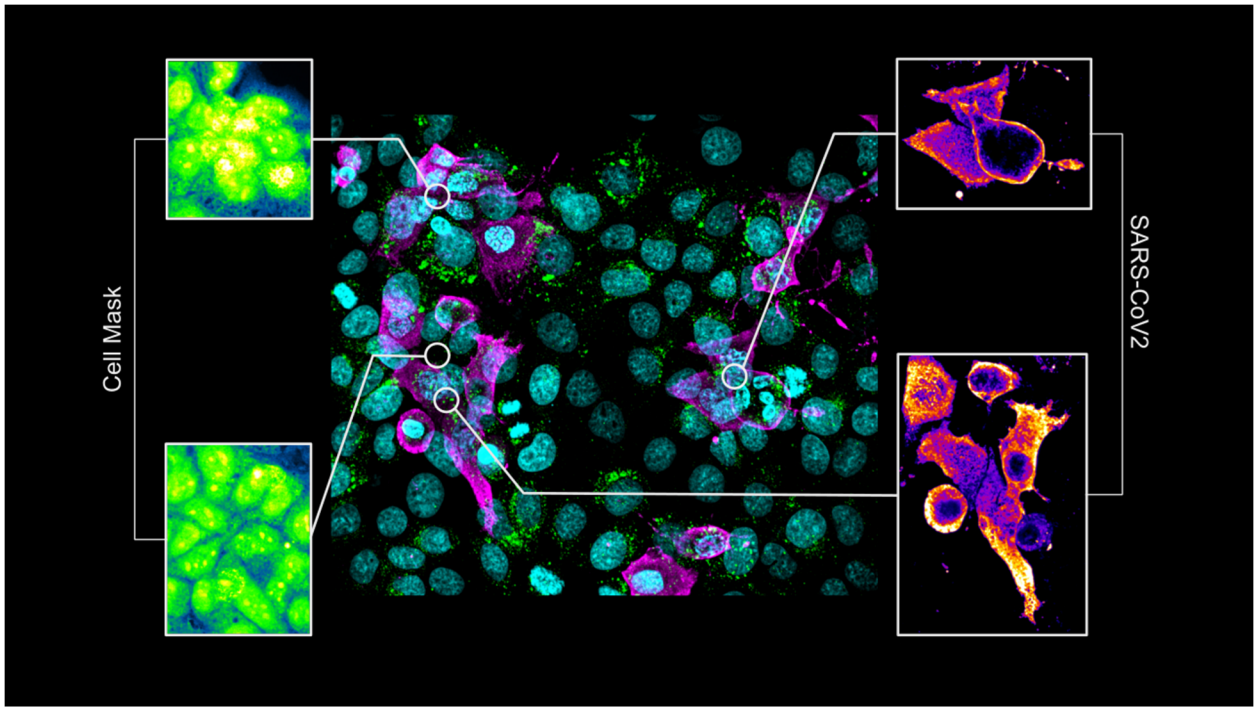

Figure 1. Morphological profiling of SARS-CoV-2 infected Huh-7 cells (MOI of 0.2 for 48 hrs). Center image: representative field with nuclei (cyan), neutral lipids (green), and SARS-CoV-2 NP protein (magenta). Through feature extraction key traits of SARS-CoV-2 infection were characterized with multinucleated syncytia (top left) and abundant nucleoli (bottom left) from HCS CellMask Orange channel. Cell viral compartmentalization (top right) with cytoplasmic protrusions (bottom right) from SARS-CoV-2 NP channel. Representative image was acquired on a Yokogawa CQ1 high-content imager and visualized with Fiji ImageJ package.

bioRxiv preprint doi: https://doi.org/10.1101/2020.05.27.117184; this version posted May 27, 2020. The copyright holder for this preprint (which was not certified by peer review) is the author/funder, who has granted bioRxiv a license to display the preprint in perpetuity. It is made available under aCC-BY-NC-ND 4.0 International license.

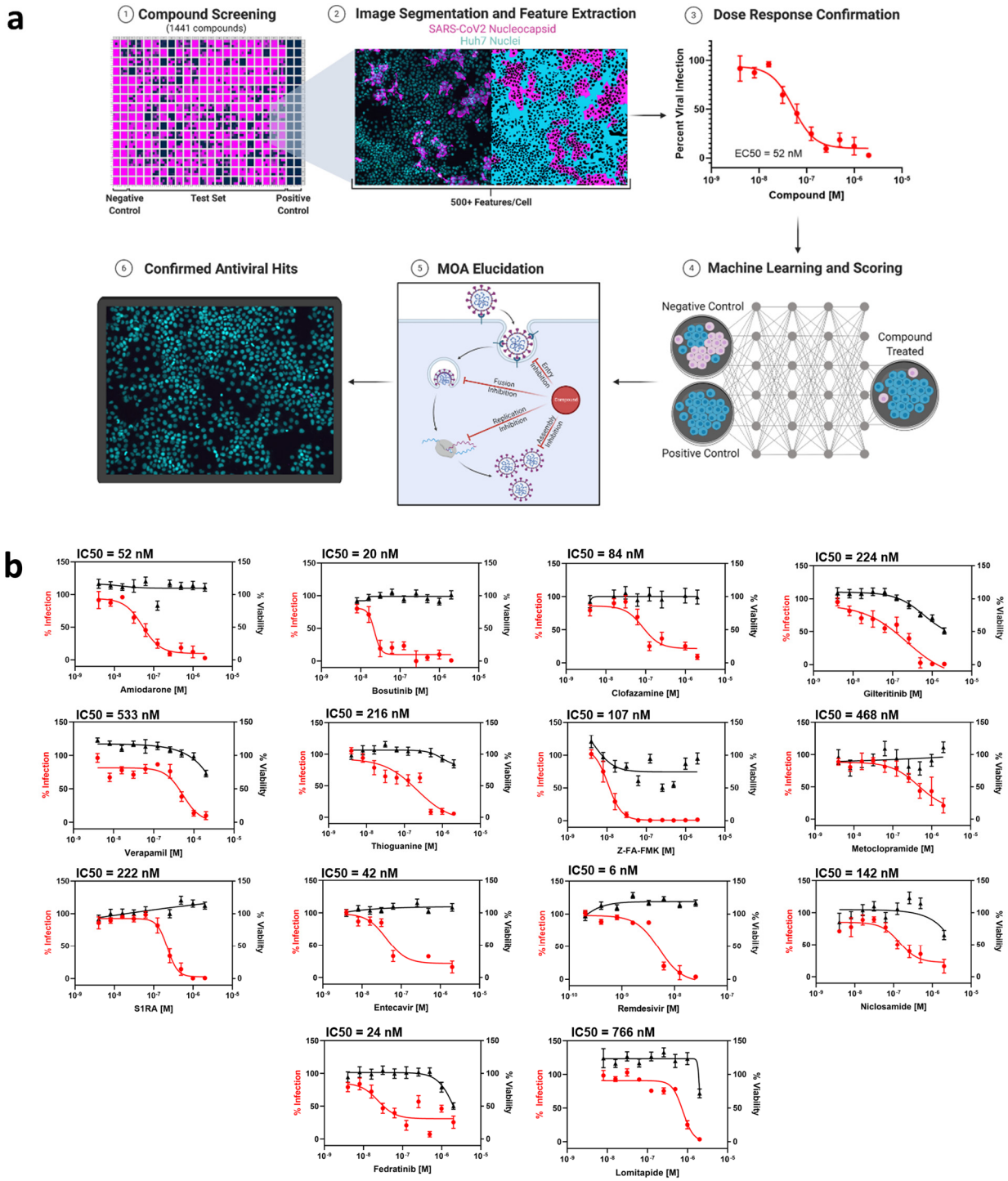

Figure 2. a) Schematic representation of the anti-SARS-CoV-2 therapy discovery effort. 1) Compounds are administered to cells cultured on 384-well plates infected with SARS-CoV-2. Each plate contains 24 negative (infected) and 24 positive (non-infected) control wells to control for plate-to-plate variation. 2) Cells are fixed, stained, and imaged. Images are analyzed through

bioRxiv preprint doi: https://doi.org/10.1101/2020.05.27.117184; this version posted May 27, 2020. The copyright holder for this preprint (which was not certified by peer review) is the author/funder, who has granted bioRxiv a license to display the preprint in perpetuity. It is made available under aCC-BY-NC-ND 4.0 International license.

a Cell Profiler-based pipeline which segments nuclei, cell boundaries, neutral lipid content and viral syncytia formation while extracting features of these cellular compartments. 3) Dose-response curves are calculated through multivariate-analysis to define per-image viral infectivity 4) Machine learning models are built around positive and negative control wells based on extracted features and applied to each drug condition. 5) Models inform on individual compound mode(s) of antiviral action through obtained features 6) confirmed antiviral hits; b) Dose-response curves of 15 hits of the drug screening. Graphs represent median SEM of 10-point 1:2 dilution series of selected compounds for N=3 biological replicates. IC_{50} were calculated based on normalization to the control and after fitting in GraphPad Prism.

bioRxiv preprint doi: https://doi.org/10.1101/2020.05.27.117184; this version posted May 27, 2020. The copyright holder for this preprint (which was not certified by peer review) is the author/funder, who has granted bioRxiv a license to display the preprint in perpetuity. It is made available under aCC-BY-NC-ND 4.0 International license.

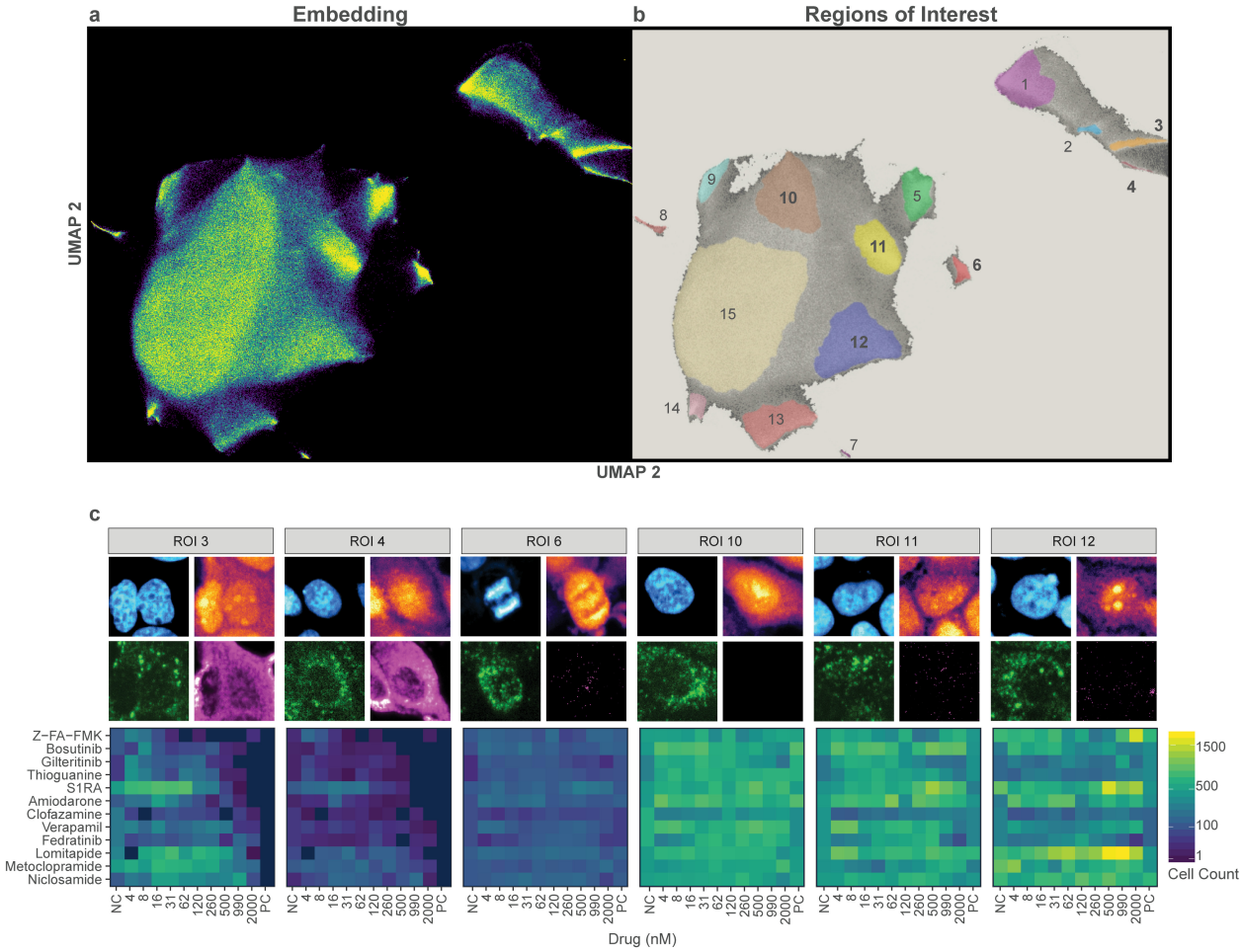

Figure 3. a) 2 dimensional UMAP embedding of two million individual cells by 379 morphological features consisting of uninfected (PC), infected (NC), or infected and treated with 12 FDA approved and clinical candidate drug screening hits across 10 doses. b) Cluster regions of interest (ROI) in the UMAP are highlighted including infected syncytial (ROI 3) and isolated (ROI 4) cells and non-infected mitotic (ROI 6), normal (ROI 10), scattered lipid (ROI 11), and cytoplasm punctate (ROI 12) cells. c) For six ROIs, a representative cell is shown by nuclear (upper-left), cell boundary (upper-right), neutral lipid (lower-left), and SARS-CoV-2 nucleocapsid (lower-right) channels. Below, the cell count across each treatment and dose is shown as a heat-map, where the dose-responsive behavior for ROIs 3 and 4 are visible.

bioRxiv preprint doi: https://doi.org/10.1101/2020.05.27.117184; this version posted May 27, 2020. The copyright holder for this preprint (which was not certified by peer review) is the author/funder, who has granted bioRxiv a license to display the preprint in perpetuity. It is made available under aCC-BY-NC-ND 4.0 International license.

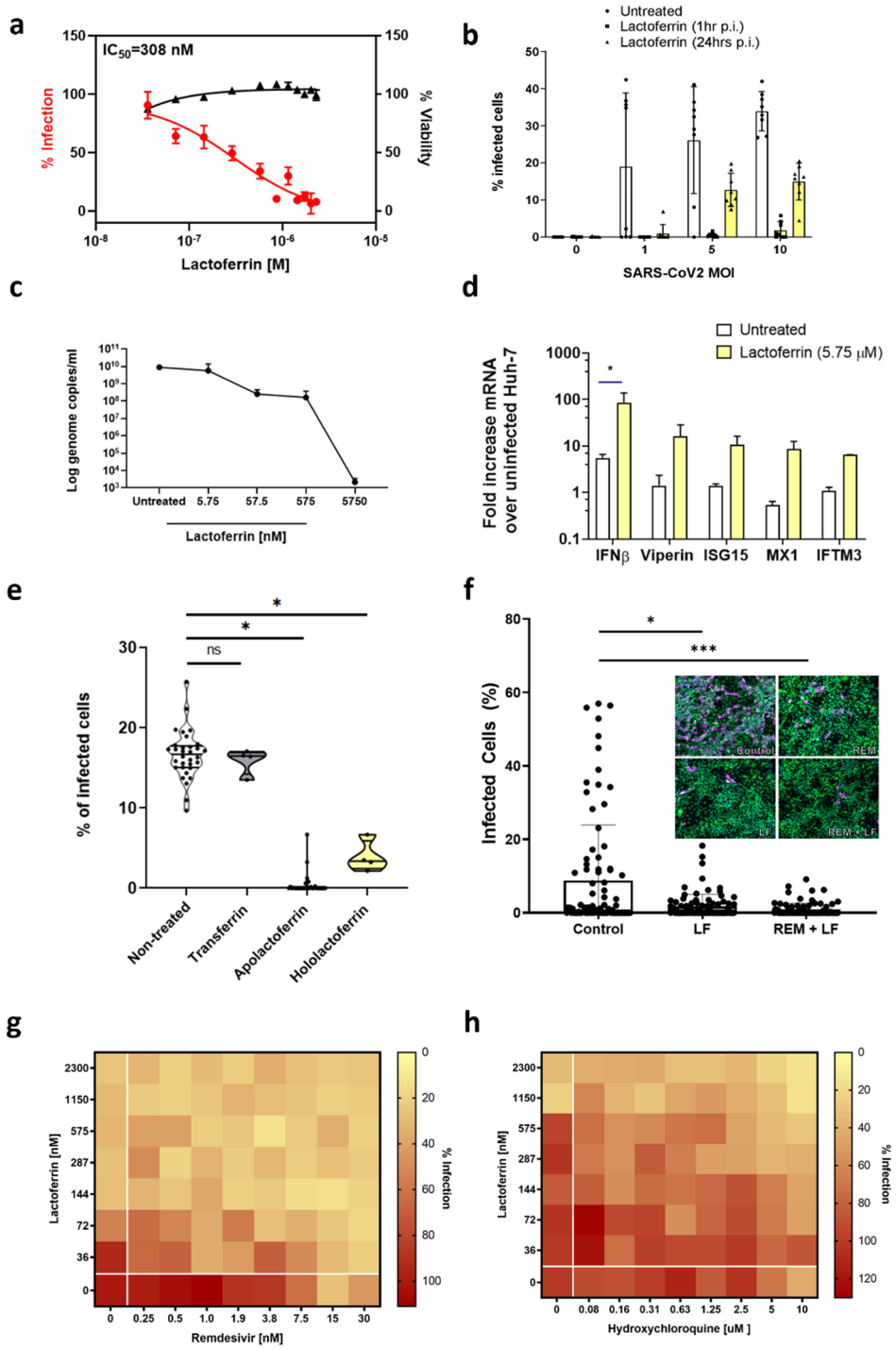

Figure 4. Lactoferrin blocks SARS-CoV-2 replication at different stages of the viral cycle. a) Huh-7 cells were treated with lactoferrin (0 to 2.3 μM) and infected with SARS-CoV-2 (MOI of 0.2) in a 384-well plate. Plates were imaged using automated fluorescence microscopy and processed

bioRxiv preprint doi: https://doi.org/10.1101/2020.05.27.117184; this version posted May 27, 2020. The copyright holder for this preprint (which was not certified by peer review) is the author/funder, who has granted bioRxiv a license to display the preprint in perpetuity. It is made available under aCC-BY-NC-ND 4.0 International license.

using our image analysis pipeline to determine percent viral inhibition. Graph indicates a dose-response (RED, IC_{50} = 308 μM). Cell viability is depicted in black. b) Huh-7 were infected with SARS-CoV-2 (MOI of 1, 5 and 10; MOI of 0 indicates non-infected cells) and treated with 2.3 μM of Lactoferrin at 1 and 24hrs p.i. Bars indicate the percentage of infected cells in different conditions. Data is an average of 8 replicates. Statistical significance determined using multiple T-test with the Bonferroni-Dunn method, with alpha = 0.05. Except for MOI of 0, all conditions (Untreated *vs* Lactoferrin, 1 hr or Untreated *vs* Lactoferrin, 24 hr) differ at P<0.0001. c-d) $2.5x10^4$ Huh-7 cells were infected with SARS-CoV-2 at MOI of 0.2. 48 hrs p.i., cells were harvested and RNA was extracted. Viral genome copies were calculated with an absolute quantification method (standard curve) (c) and mRNA levels of cellular IFNβ, MX1, ISG15 and IFITM3 (d) were calculated with ΔΔCt over non-infected Huh-7. Data are average, SD of N=2 biological replicates with n=3 technical replicates each. Statistical significance determined using multiple T-test with the Bonferroni-Dunn method, with alpha = 0.05. *P<0.001. e) Percentage of SARS-CoV-2 infected Huh-7 cells upon treatment with apolactoferrin, hololactoferrin, and transferrin at a concentration of 2.3 μM. f) Percentage of infected iAEC2 48 hrs p.i. at MOI of 10 upon treatment with remdesivir (50 nM), lactoferrin (1.2μM), and remdesivir/lactoferrin (25 nM/600 nM) combination treatment. Error bars shown are SEM. Significance was calculated using Kruskal-Wallis test followed by Dunn's multiple comparison test. *P<0.05 and ***P<0.001. g) and h) 2-dimensional dose response heat maps of lactoferrin (0 to 2.3 μM) in combination with remdesivir and hydroxychloroquine (0 to 30 nM and 0 to 10 μM, respectively). Remdesivir combination was evaluated with a 0.2 MOI and HCQ was evaluated with a MOI of 10 leading to a relative shift in lactoferrin potency.

bioRxiv preprint doi: https://doi.org/10.1101/2020.05.27.117184; this version posted May 27, 2020. The copyright holder for this preprint (which was not certified by peer review) is the author/funder, who has granted bioRxiv a license to display the preprint in perpetuity. It is made available under aCC-BY-NC-ND 4.0 International license.

SUPPLEMENTARY INFORMATION

Supplementary Figure 1: Screening assay optimization

Supplementary Figure 2: Compounds exacerbating SARS-CoV2 infection

Supplementary Figure 3: Features of UMAP regions of interest (ROI)

Supplementary Figure 4: Combinatory effects of remdesivir and hydroxycholoroquine with lactoferrin

Supplementary Table 1: Compound Deep Dives

Supplementary File 1: Compound library details

Supplementary File 2: 3D reconstruction video of infected cells

bioRxiv preprint doi: https://doi.org/10.1101/2020.05.27.117184; this version posted May 27, 2020. The copyright holder for this preprint (which was not certified by peer review) is the author/funder, who has granted bioRxiv a license to display the preprint in perpetuity. It is made available under aCC-BY-NC-ND 4.0 International license.

REFERENCES

1. Xiao, F. *et al.* Evidence for Gastrointestinal Infection of SARS-CoV-2. *Gastroenterology* (2020). doi:10.1053/j.gastro.2020.02.055
2. Lin, L. *et al.* Gastrointestinal symptoms of 95 cases with SARS-CoV-2 infection. *Gut* (2020). doi:10.1136/gutjnl-2020-321013
3. Avula, A. *et al.* COVID-19 presenting as stroke. *Brain. Behav. Immun.* (2020). doi:10.1016/j.bbi.2020.04.077
4. Kochi, A. N., Tagliari, A. P., Forleo, G. B., Fassini, G. M. & Tondo, C. Cardiac and arrhythmic complications in patients with COVID-19. *Journal of Cardiovascular Electrophysiology* (2020). doi:10.1111/jce.14479
5. Mulangu, S. *et al.* A randomized, controlled trial of Ebola virus disease therapeutics. *N. Engl. J. Med.* (2019). doi:10.1056/NEJMoa1910993
6. Oprea, T. I. *et al.* Drug repurposing from an academic perspective. *Drug Discovery Today: Therapeutic Strategies* (2011). doi:10.1016/j.ddstr.2011.10.002
7. Chu, H. *et al.* Comparative tropism, replication kinetics, and cell damage profiling of SARS-CoV-2 and SARS-CoV with implications for clinical manifestations, transmissibility, and laboratory studies of COVID-19: an observational study. *The Lancet Microbe* (2020). doi:10.1016/s2666-5247(20)30004-5
8. Hoffmann, M. *et al.* SARS-CoV-2 Cell Entry Depends on ACE2 and TMPRSS2 and Is Blocked by a Clinically Proven Protease Inhibitor. *Cell* (2020). doi:10.1016/j.cell.2020.02.052
9. Riva, L. *et al.* A Large-scale Drug Repositioning Survey for SARS-CoV-2 Antivirals. *bioRxiv* (2020). doi:10.1101/2020.04.16.044016
10. Katie Heiser *et al.* Identification of potential treatments for COVID-19 through artificial intelligence enabled phenomic analysis of human cells infected with SARS-CoV-2. *bioRxiv* (2020). doi:10.1101/2020.04.21.054387

bioRxiv preprint doi: https://doi.org/10.1101/2020.05.27.117184; this version posted May 27, 2020. The copyright holder for this preprint (which was not certified by peer review) is the author/funder, who has granted bioRxiv a license to display the preprint in perpetuity. It is made available under aCC-BY-NC-ND 4.0 International license.

11. Jeon, S. *et al.* Identification of antiviral drug candidates against SARS-CoV-2 from FDA-approved drugs. *Antimicrob. Agents Chemother.* (2020). doi:10.1128/AAC.00819-20

12. McInnes, L., Healy, J., Saul, N. & Großberger, L. UMAP: Uniform Manifold Approximation and Projection. *J. Open Source Softw.* (2018). doi:10.21105/joss.00861

13. Lang, J. *et al.* Inhibition of SARS pseudovirus cell entry by lactoferrin binding to heparan sulfate proteoglycans. *PLoS One* (2011). doi:10.1371/journal.pone.0023710

14. Siqueiros-Cendón, T. *et al.* Immunomodulatory effects of lactoferrin. *Acta Pharmacologica Sinica* (2014). doi:10.1038/aps.2013.200

15. Jacob, A. *et al.* Derivation of self-renewing lung alveolar epithelial type II cells from human pluripotent stem cells. *Nat. Protoc.* (2019). doi:10.1038/s41596-019-0220-0

16. Hurley, K. *et al.* Reconstructed Single-Cell Fate Trajectories Define Lineage Plasticity Windows during Differentiation of Human PSC-Derived Distal Lung Progenitors. *Cell Stem Cell* (2020). doi:10.1016/j.stem.2019.12.009

17. Yeni, P. Update on HAART in HIV. in *Journal of Hepatology* (2006). doi:10.1016/j.jhep.2005.11.021

18. Evans, W. E. Pharmacogenetics of Thiopurine S-Methyltransferase and Thiopurine Therapy. in *Therapeutic Drug Monitoring* (2004). doi:10.1097/00007691-200404000-00018

19. Arbiser, J. L. & Moschella, S. L. Clofazimine: A review of its medical uses and mechanisms of action. *Journal of the American Academy of Dermatology* (1995). doi:10.1016/0190-9622(95)90134-5

20. Alghamdi, S., Leoncikas, V., Plant, K. E. & Plant, N. J. Synergistic interaction between lipid-loading and doxorubicin exposure in Huh7 hepatoma cells results in enhanced cytotoxicity and cellular oxidative stress: Implications for acute and chronic care of obese cancer patients. *Toxicol. Res. (Camb).* (2015). doi:10.1039/c5tx00173k

21. Hibbs, A. M. & Lorch, S. A. Metoclopramide for the treatment of gastroesophageal reflux

bioRxiv preprint doi: https://doi.org/10.1101/2020.05.27.117184; this version posted May 27, 2020. The copyright holder for this preprint (which was not certified by peer review) is the author/funder, who has granted bioRxiv a license to display the preprint in perpetuity. It is made available under aCC-BY-NC-ND 4.0 International license.

disease in infants: A systematic review. *Pediatrics* (2006). doi:10.1542/peds.2005-2664

22. Hajifathalian, K. *et al.* SARS-COV-2 infection (coronavirus disease 2019) for the gastrointestinal consultant. *World J. Gastroenterol.* (2020). doi:10.3748/wjg.v26.i14.1546

23. Roscow, O., Ganassin, R., Garver, K. & Polinski, M. Z-FA-FMK demonstrates differential inhibition of aquatic orthoreovirus (PRV), aquareovirus (CSRV), and rhabdovirus (IHNV) replication. *Virus Res.* (2018). doi:10.1016/j.virusres.2017.11.024

24. Ou, X. *et al.* Characterization of spike glycoprotein of SARS-CoV-2 on virus entry and its immune cross-reactivity with SARS-CoV. *Nat. Commun.* (2020). doi:10.1038/s41467-020-15562-9

25. Pardanani, A. *et al.* TG101209, a small molecule JAK2-selective kinase inhibitor potently inhibits myeloproliferative disorder-associated JAK2V617F and MPLW515L/K mutations. *Leukemia* (2007). doi:10.1038/sj.leu.2404750

26. Wu, D. & Yang, X. O. TH17 responses in cytokine storm of COVID-19: An emerging target of JAK2 inhibitor Fedratinib. *J. Microbiol. Immunol. Infect.* (2020). doi:10.1016/j.jmii.2020.03.005

27. Zhang, W. *et al.* The use of anti-inflammatory drugs in the treatment of people with severe coronavirus disease 2019 (COVID-19): The experience of clinical immunologists from China. *Clinical Immunology* (2020). doi:10.1016/j.clim.2020.108393

28. Stebbing, J. *et al.* COVID-19: combining antiviral and anti-inflammatory treatments. *The Lancet Infectious Diseases* (2020). doi:10.1016/S1473-3099(20)30132-8

29. Treatment of Moderate to Severe Coronavirus Disease (COVID-19) in Hospitalized Patients. (2020). Available at: https://clinicaltrials.gov/ct2/show/NCT04321993.

30. Delprat, B., Crouzier, L., Su, T. P. & Maurice, T. At the Crossing of ER Stress and MAMs: A Key Role of Sigma-1 Receptor? in *Advances in Experimental Medicine and Biology* (2020). doi:10.1007/978-3-030-12457-1_28

31. Friesland, M., Mingorance, L., Chung, J., Chisari, F. V. & Gastaminza, P. Sigma-1

bioRxiv preprint doi: https://doi.org/10.1101/2020.05.27.117184; this version posted May 27, 2020. The copyright holder for this preprint (which was not certified by peer review) is the author/funder, who has granted bioRxiv a license to display the preprint in perpetuity. It is made available under aCC-BY-NC-ND 4.0 International license.

Receptor Regulates Early Steps of Viral RNA Replication at the Onset of Hepatitis C Virus Infection. *J. Virol.* (2013). doi:10.1128/jvi.03557-12

32. Fung, T. S. & Liu, D. X. Coronavirus infection, ER stress, apoptosis and innate immunity. *Frontiers in Microbiology* (2014). doi:10.3389/fmicb.2014.00296

33. Moebius, F. F., Reiter, R. J., Hanner, M. & Glossmann, H. High affinity of sigma1-binding sites for sterol isomerization inhibitors: Evidence for a pharmacological relationship with the yeast sterol C8-C7 isomerase. *Br. J. Pharmacol.* (1997). doi:10.1038/sj.bjp.0701079

34. Díaz, J. L. *et al.* Synthesis and biological evaluation of the 1-arylpyrazole class of σ1 receptor antagonists: Identification of 4-{2-[5-methyl-1- (naphthalen-2-yl)-1H-pyrazol-3-yloxy]ethyl}morpholine (S1RA, E-52862). *J. Med. Chem.* (2012). doi:10.1021/jm3007323

35. Torres, V. *et al.* QT prolongation and the antiarrhythmic efficacy of amiodarone. *J. Am. Coll. Cardiol.* (1986). doi:10.1016/S0735-1097(86)80272-8

36. Vidal-Torres, A. *et al.* Effects of the selective sigma-1 receptor antagonist S1RA on formalin-induced pain behavior and neurotransmitter release in the spinal cord in rats. *J. Neurochem.* (2014). doi:10.1111/jnc.12648

37. Gris, G. *et al.* The selective sigma-1 receptor antagonist E-52862 attenuates neuropathic pain of different aetiology in rats. *Sci. Rep.* (2016). doi:10.1038/srep24591

38. Gordon, D. E. *et al.* A SARS-CoV-2 protein interaction map reveals targets for drug repurposing. *Nature* (2020). doi:10.1038/s41586-020-2286-9

39. Reghunathan, R. *et al.* Expression profile of immune response genes in patients with severe acute respiratory syndrome. *BMC Immunol.* (2005). doi:10.1186/1471-2172-6-2

40. Cutone, A. *et al.* Lactoferrin prevents LPS-induced decrease of the iron exporter ferroportin in human monocytes/macrophages. *BioMetals* (2014). doi:10.1007/s10534-014-9742-7

41. Conti, P. *et al.* Induction of pro-inflammatory cytokines (IL-1 and IL-6) and lung inflammation by COVID-19: anti-inflammatory strategies. *Journal of biological regulators*

bioRxiv preprint doi: https://doi.org/10.1101/2020.05.27.117184; this version posted May 27, 2020. The copyright holder for this preprint (which was not certified by peer review) is the author/funder, who has granted bioRxiv a license to display the preprint in perpetuity. It is made available under aCC-BY-NC-ND 4.0 International license.

and homeostatic agents (2020). doi:10.23812/CONTI-E.

42. Lagunas-Rangel, F. A. & Chávez-Valencia, V. High IL-6/IFN-γ ratio could be associated with severe disease in COVID-19 patients. *Journal of Medical Virology* (2020). doi:10.1002/jmv.25900

43. Han, C. *et al.* Digestive Symptoms in COVID-19 Patients With Mild Disease Severity: Clinical Presentation, Stool Viral RNA Testing, and Outcomes. *Am. J. Gastroenterol.* (2020). doi:10.14309/ajg.0000000000000664

44. Oda, H. *et al.* Antiviral Effects of Bovine Lactoferrin on Human Norovirus. *Biochem. Cell Biol.* (2020). doi:10.1139/bcb-2020-0035

45. Mohamed, J. A. *et al.* A Novel Single-Nucleotide Polymorphism in the Lactoferrin Gene Is Associated with Susceptibility to Diarrhea in North American Travelers to Mexico. *Clin. Infect. Dis.* (2007). doi:10.1086/512199

46. Gu, J., Han, B. & Wang, J. COVID-19: Gastrointestinal Manifestations and Potential Fecal–Oral Transmission. *Gastroenterology* (2020). doi:10.1053/j.gastro.2020.02.054

47. Hung, I. F.-N. *et al.* Triple combination of interferon beta-1b, lopinavir–ritonavir, and ribavirin in the treatment of patients admitted to hospital with COVID-19: an open-label, randomised, phase 2 trial. *Lancet* (2020). doi:10.1016/s0140-6736(20)31042-4

48. Berthold, M. R. *et al.* KNIME: The konstanz information miner. in *4th International Industrial Simulation Conference 2006, ISC 2006* (2006). doi:10.1007/978-3-540-78246-9_38

49. Stevens, J.-L., Rudiger, P. & Bednar, J. HoloViews: Building Complex Visualizations Easily for Reproducible Science. in *Proceedings of the 14th Python in Science Conference* (2015). doi:10.25080/majora-7b98e3ed-00a